

Detecting Induced $p \pm ip$ Pairing at the Al-InAs Interface with a Quantum Microwave Circuit

D. Phan¹, J. Senior¹, A. Ghazaryan¹, M. Hatefipour², W. M. Strickland², J. Shabani²,
M. Serbyn¹ and A. P. Higginbotham^{1,*}

¹IST Austria, Am Campus 1, 3400 Klosterneuburg, Austria

²Department of Physics, New York University, New York, New York 10003, USA

(Received 14 October 2021; revised 15 December 2021; accepted 31 January 2022; published 11 March 2022)

Superconductor-semiconductor hybrid devices are at the heart of several proposed approaches to quantum information processing, but their basic properties remain to be understood. We embed a two-dimensional Al-InAs hybrid system in a resonant microwave circuit, probing the breakdown of superconductivity due to an applied magnetic field. We find a fingerprint from the two-component nature of the hybrid system, and quantitatively compare with a theory that includes the contribution of intraband $p \pm ip$ pairing in the InAs, as well as the emergence of Bogoliubov-Fermi surfaces due to magnetic field. Separately resolving the Al and InAs contributions allows us to determine the carrier density and mobility in the InAs.

DOI: 10.1103/PhysRevLett.128.107701

Hybrids of superconducting and semiconducting materials are under investigation as platforms for integrated superconducting devices [1,2], superconducting qubits [3–6], and engineered p -wave superconductivity [7–10]. Hindering progress toward these goals, basic semiconductor properties such as carrier density, mobility, and induced pairing are currently inaccessible because the superconductor acts as a perfectly conductive shunt. This problem is especially acute in the ongoing effort to conclusively identify Majorana modes [11–20]. Because of the bulk-boundary correspondence, the presence of these modes should be controlled by bulk, as yet undetermined, semiconductor parameters. In particular, depending on parameter values, the application of a magnetic field can result in transitions to the normal state [21–23], partial Bogoliubov-Fermi surfaces [24], gapless p_x phases [25], or chiral p -wave phases with Majorana modes [25–30].

In this Letter, we experimentally study induced superconductivity in a two-dimensional Al-InAs hybrid system using a resonant microwave circuit. Above a characteristic field we discover anisotropic suppression of superfluid density and enhanced dissipation, consistent with a picture of two fully gapped, intraband $p \pm ip$ superconductors transitioning to partial Bogoliubov-Fermi surfaces. Observation of this transition allows for the characterization of key system properties such as induced pairing, carrier density, and carrier mobility. We therefore demonstrate the first evidence of two-dimensional induced p -wave pairing, the emergence of Bogoliubov-Fermi surfaces, and a general method for characterizing otherwise invisible properties of superconductor-semiconductor hybrid devices.

The basic picture of proximity effect in Al-InAs is presented in Fig. 1. An aluminum layer with a spin-degenerate Fermi surface is strongly coupled to a high-mobility InAs two-dimensional electron gas. InAs has a pair of spin-orbit coupled Fermi surfaces which results in $p \pm ip$ intraband pairing of the form $\Delta(k_x \pm ik_y)/|k|$ for pure Rashba spin-orbit interaction, where k is the momentum at the Fermi surface labeled by \pm [7,25]. This pairing holds a special importance because a state with single,

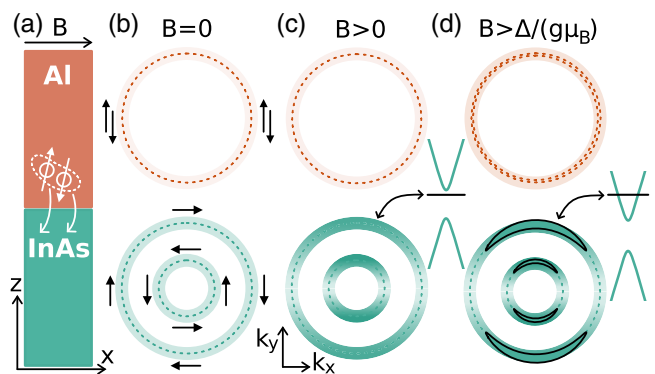


FIG. 1. (a) Physical picture of proximity effect between Al in InAs. Field direction, B , indicated. (b) Al has a spin-degenerate Fermi surface gapped by superconductivity (orange). InAs has two spin-orbit coupled Fermi surfaces with intraband $p \pm ip$ pairing (green). (c) Magnetic field anisotropically reduces InAs gap (color intensity). Hyperbolas indicate quasiparticles' dispersion. Black line indicates chemical potential. (d) For $B > \Delta/(g\mu_B)$ the InAs gap closes in isolated regions, forming connected arcs of zero-energy electronlike and holelike quasiparticles, known as Bogoliubov-Fermi surfaces.

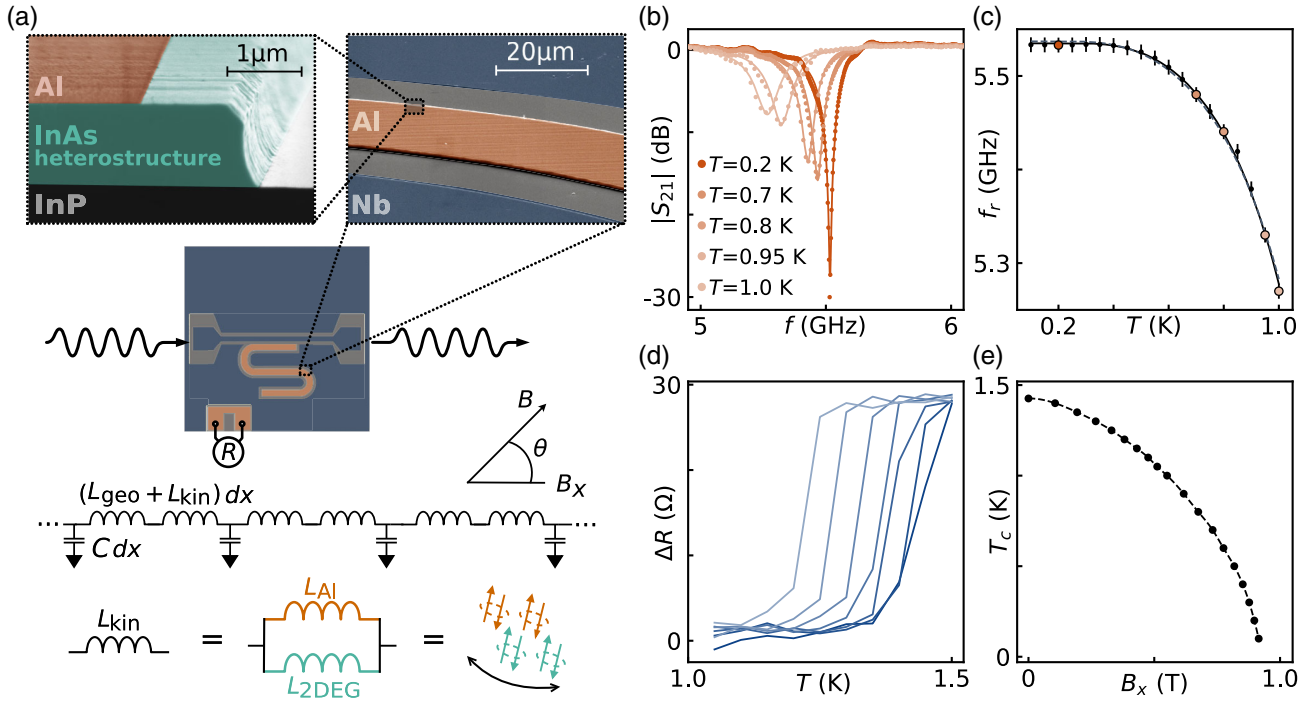


FIG. 2. (a) False-color scanning-electron micrographs of an example Al-InAs device. The InAs heterostructure houses a two-dimensional electron gas (top). Schematic of the chip layout with microwave resonator, transport device allowing for measurement of resistance R , magnetic-field angle θ (middle). Transmission-line model with geometric inductance L_{geo} and kinetic inductance L_{kin} , which receives a contribution from the Al and from the InAs. (b) Microwave transmission S_{21} as a function of frequency, measured for different cryostat temperatures. Solid lines are fits using method of Ref. [58]. (c) Resonant frequency f_r extracted from (a) versus cryostat temperature T , colored points match like-colored traces in (b). Solid line is a fit to s -wave theory including disorder ($c_p = 0$), and dashed line is a fit to the two-component model. (d) Resistance R vs temperature T . Curves from right to left have B_x uniformly increasing from 0 to 0.36 T. A 15Ω overall offset has been subtracted from the data. (e) Critical temperature as a function of x -oriented magnetic field B_x . Points joined by an interpolating function, used for smoothly estimating $T_c(B)$ in the pair-breaking numerical fit.

chiral $p_x + ip_y$ pairing is topologically nontrivial, and therefore capable of hosting Majorana modes [31]. Application of an in plane magnetic field probes the nature of the induced pairing. For weak spin-orbit coupling, interband s -wave pairing quickly emerges [25,32], and the system eventually transitions to an isotropic normal state [23]. In contrast, strong spin-orbit coupling makes the $p \pm ip$ pairing robust. The magnetic field then generates anisotropic suppression of the induced gap, eventually causing the emergence of Bogoliubov-Fermi surfaces [24]. Bogoliubov-Fermi surfaces, however, may be subject to an instability that was explored in related systems [33–37]. Thus the presence of $p \pm ip$ pairing qualitatively affects the response of superconductivity to in plane magnetic fields, motivating the present study.

In order to probe the effect of a magnetic field on induced superconductivity, we construct a half wave coplanar waveguide resonator with a center pin made from an Al-InAs superconductor-semiconductor heterostructure [38–40], shown in Fig. 2(a) with more material details in the Supplemental Material [41]. The resonant frequency of this circuit is altered by the condensate kinetic

inductance, which is inversely proportional to superfluid density ρ_{SF} [56,57]. The emergence of Bogoliubov-Fermi arcs is expected to deplete the contribution of InAs to ρ_{SF} , and thus alter the circuit resonant frequency.

The resonator is modeled as a distributed LC circuit consisting of infinitesimal inductances and capacitances extending over the resonator length l [Fig. 2(b)]. The circuit's resonant frequency f_r depends on the geometric resonance f_{geo} and kinetic contribution f_{kin} added in inverse quadrature [59],

$$\frac{1}{f_r^2} = \frac{1}{f_{\text{geo}}^2} + \frac{1}{f_{\text{kin}}^2}, \quad (1)$$

where $f_{\text{geo}} = (2l\sqrt{L_{\text{geo}}C})^{-1}$ and $f_{\text{kin}} = (2l\sqrt{L_{\text{kin}}C})^{-1}$. The inductance (capacitance) per unit length L_{geo} (C) is determined by geometry. In contrast, the kinetic inductance, L_{kin} , probes the superconducting condensate and has two contributions,

$$f_{\text{kin}}^2 = c_s n_s + c_p n_p, \quad (2)$$

where n_s (n_p) are normalized superfluid densities associated with the contribution of s -wave Al ($p \pm ip$ InAs) superconductors. Dimensionless densities $n_{s,p}$ are normalized to zero-temperature and zero-field limit values, while the parameters c_s , c_p encode the zero-temperature and zero-field value of superfluid density and geometry of the sample, thus giving access to the properties of corresponding material. The function n_s accounts for the depairing effect of the magnetic field and depletion of superfluid density due to thermally activated quasiparticles in Al. The function n_p quantifies the depletion of superfluid density in InAs with $p \pm ip$ pairing (assuming high-density and strong spin-orbit coupling, so that interband pairing can be ignored) due to the emergence of Bogoliubov-Fermi surfaces for sufficiently strong magnetic fields. We treat the resonator as probing only the x component of n_p because 80% of the resonator is oriented in the x direction.

Microwave access is provided by capacitively coupling the resonator to a transmission line, allowing the transmission coefficient S_{21} to be measured. The device is placed in a magnetic field with the axis B_x parallel to the transmission line, which can be rotated by an angle θ in the $B_x - B_y$ plane. A cofabricated device is used for transport characterization. Measuring circuit transmission at $B = 0$ and $T = 0.1$ K, a prominent resonance is observed as a dip in the total transmission at a frequency $f_r \approx 5.53$ GHz [Fig. 2(b)]. Increasing the cryostat temperature T , a frequency down-shift and reduction in quality factor is observed. As shown in Fig. 2(c), the $B = 0$ temperature dependence of f_r is nearly identical for the single-component s -wave superconductor (solid curve) and a full two-component model that includes the contribution of $p \pm ip$ pairing in the InAs (dashed curve). To resolve the contribution of the InAs, it is therefore necessary to apply a magnetic field, where one expects large qualitative differences from the standard response of a disordered s -wave superconductor (see Fig. 1).

The measured dependence of resonant frequency on the value of the in plane field is shown in Fig. 3(a), where careful cancellation of the perpendicular field was ensured [41]. Increasing the magnetic field from zero initially causes only a slight decrease in f_r , which is qualitatively consistent with the pair-breaking effect of the magnetic field on aluminum. In fact, the black line in Fig. 3(a) shows the prediction of the pair-breaking theory of a single-component s -wave superconductor. This theory utilizes the suppression of critical temperature with the in plane magnetic field, $T_c(B)/T_c(0)$, measured on a cofabricated transport device [Fig. 2(e)], and therefore has no free fitting parameters. Crucially, the resonator response decreases abruptly at a characteristic field scale $B^* \sim 0.33$ T, in violation of the expectations from pair breaking in pure aluminum.

The decrease of resonator frequency caused by a rapid suppression of superfluid density can be understood by

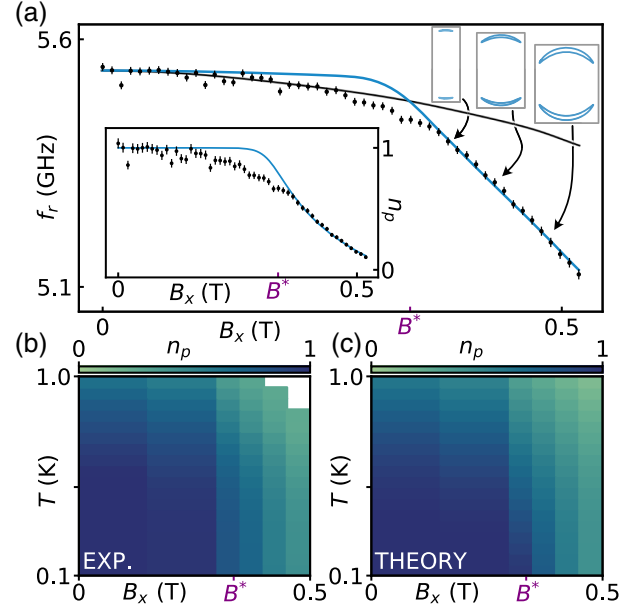


FIG. 3. (a) Points show measured resonant frequency f_r versus B_x . Lines correspond to single-component s -wave superconductor model, Eq. (2), with $c_p = 0$ (black) and to the two-component model with nonzero c_s and c_p (blue). Two-component model Bogoliubov-Fermi surfaces are indicated. Fit to two-component model is performed by simultaneously fitting the linear region of the data for $B > B^*$ and the temperature dependence $f_r(T, B = 0)$ in Fig. 2(c). Inset shows inferred superfluid density n_p with the same x axis as the main figure [41]. (b) Experimental inference of n_p versus magnetic field and temperature. (c) Theoretical prediction for n_p versus magnetic field and temperature from two-component model.

considering the two-component nature of the superconducting condensate. The model in Eq. (2) that incorporates superfluid density contribution of both Al and InAs is able to adequately capture the full range of frequency behavior [blue line in Fig. 3(a)]: it accounts for the conventional behavior at $B < B^*$, corresponding to a fully gapped p -wave component, and shows the rapid downturn at $B > B^*$, corresponding to the emergence of Bogoliubov-Fermi surfaces in the InAs. The model struggles in the regime $B \sim B^*$ because it does not incorporate the role of disorder in the InAs, and therefore underestimates orbital pair-breaking effects. The rapid onset of the frequency suppression with an in plane field not only provides experimental evidence for the $p \pm ip$ proximity-induced pairing in the InAs semiconductor, but also allows *in situ* characterization of InAs material properties.

Access to material properties is provided via the fit to the theoretical model. The fit geometric resonant frequency f_{geo} is 5.96 ± 0.01 GHz which differs by $<2\%$ with the expected value based on electromagnetic simulations and provides a strong consistency check. c_s gives the Al sheet resistance $R_{\text{Al}} = 6.7 \pm 0.2 \Omega$, in line with independent

transport measurements on MBE-grown Al thin films. c_p gives the InAs density, $4 \times 10^{13} \text{ cm}^{-2}$, which combined with the total measured sheet resistance yields an InAs mobility of $2 \times 10^4 \text{ cm}^2/(\text{Vs})$. The density is an order of magnitude larger than without Al, as expected due to band bending of InAs [60–64], whereas the mobility is comparable to the Hall value. B^* gives a bulk g factor in the x direction, $g_x = 11.2 \pm 0.2$, which is consistent with measured g factors in similar quantum wells [65–68]. These parameters give key independent information on the proximity effect in InAs. Fermi velocity mismatch between the InAs and Al ($v_{F,\text{InAs}}/v_{F,\text{Al}} \sim 3$) results in a moderate interface transparency with weak g -factor renormalization while maintaining a large induced gap due to disorder in the Al [64]. Incorporation of disorder in the InAs will cause quantitative corrections to quantities inferred from the fit.

With all parameters fixed, the normalized p -wave superfluid density can now be extracted directly from measured frequencies [Fig. 3(a) inset]. Experimentally mapping out a phase diagram for n_p in the B_x - T plane reveals that the superfluid density is depleted both by increasing the field above B^* , and by raising the temperature, in line with the theoretical model that accounts for both thermal effects and depairing in the p -wave system [Figs. 3(b) and 3(c)]. This comparison has no free parameters, which provides further strong evidence in favor of the $p \pm ip$ theory.

Motivated by the anisotropic nature of the Bogoliubov-Fermi surfaces, we have systematically studied the anisotropy of the circuit response with respect to field direction in Fig. 4(a). Measuring resonant frequency f_r as a function of field angle θ reveals a nearly isotropic response for weak values of magnetic field $B < B^*$. In contrast, for $B > B^*$ we observe strong frequency suppression in the x direction compared with the y direction, resulting in a pronounced two-lobe structure in a polar frequency plot [Fig. 4(a)], with the two prominent lobes at $\theta = \pm 90^\circ$. There is an additional hint of two smaller lobes at $\theta = 0^\circ, 180^\circ$.

In order to compare the measured field-direction-dependence of f_r with theory, we extend our model to include a g factor in the y direction g_y which is expected to differ from g_x for the present case of asymmetric (100) quantum wells [69–71]. Holding all other parameters of the theoretical model fixed, a single-parameter fit in Fig. 4(c) yields a value $g_y = 4$ [41], consistent with the expected level of in plane g -factor anisotropy [69–71], and with literature values of similar quantum wells of g factors in the range of 3–11 [65–68]. Remarkably, the addition of this single extra parameter explains the key observed anisotropic features in the dataset [Fig. 4(b)]. In particular, theory predicts two major lobes for $B > B^*$, associated with a regime where no Bogoliubov-Fermi arcs emerge due to the relatively small value of g_y , and two minor lobes associated with the dependence of arc orientation on field direction. Both the major and minor lobes predicted by the

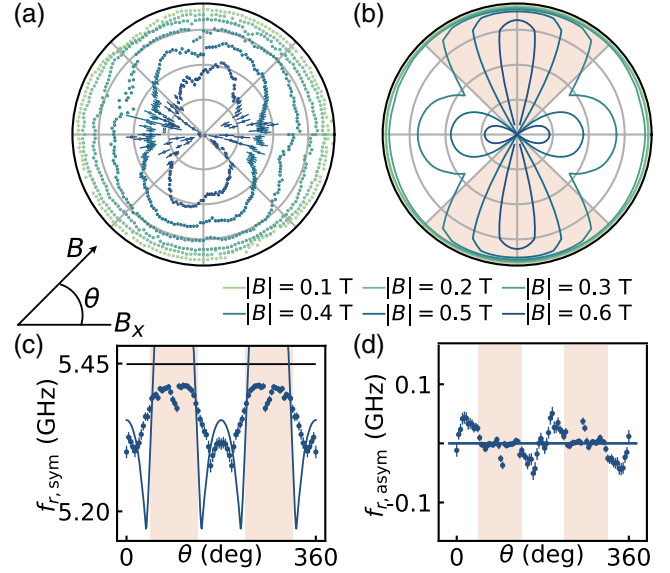


FIG. 4. (a) Measured magnetic-field orientation dependence of resonant frequency in a polar plot. Radial divisions start at $f_r = 4.8$ GHz and are in 100 MHz increments. (b) Theoretically predicted dependence of frequency on magnetic field orientation, with single free parameter fixed in (c). (c) Measured f_r at $|B| = 0.4$ T symmetrized about $\theta = 180^\circ$. Shaded regions indicate angles for which instability can play a role, which are excluded from the fit for g_y . Black curve is prediction of the s -wave pair-breaking theory. Blue curve is a single-parameter fit for B_y^* in the two-component model, which exceeds the value of the pair-breaking model because it does not include disorder. (d) Antisymmetric part of f_r vs magnetic field angle θ , blue curve is the theoretical expectation $f_{r,\text{asym}} = 0$.

theoretical model are more prominent than those in the experiment, which we attribute primarily to the theory being in the clean limit, which tends to result in an overestimated frequency for $B < B^*$, as is already apparent in Fig. 3(a). In addition in this sample there is a small odd-angle contribution to the resonant frequency [Fig. 4(d)], which is completely absent in theory. Further experimental work is needed to see if the small odd-angle contribution is experimentally robust.

Interestingly, the semiclassical model predicts that a magnetic field oriented near the y direction (shaded regions in Fig. 4), which causes the emergence of Bogoliubov-Fermi arcs aligned with the primary (x) direction of the resonator, can result in negative values of the $p \pm ip$ superfluid density ($n_p < 0$). Physically, the negative superfluid density emerges from the large density of quasiparticles due to presence of Bogoliubov-Fermi arcs, and signals an instability which has been discussed in related contexts [33–37]. We do not observe indications of the instability in the experiment, possibly due to the presence of Al layer and smearing of density of states in InAs due to disorder. The consequences of the instability for the present system remain to be understood and will be addressed in

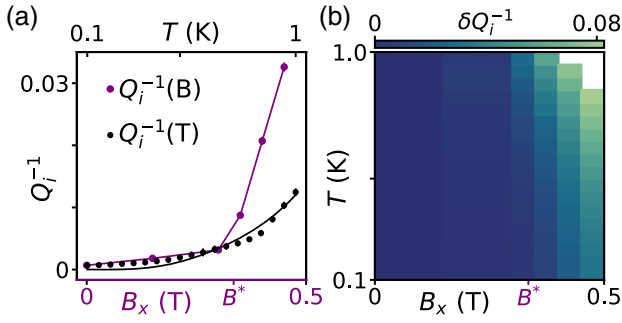


FIG. 5. (a) Dependence of inverse quality factor on magnetic field $Q_i^{-1}(B)$ at a fixed $T = 0.1$ K (purple), and dependence on temperature $Q_i^{-1}(T)$ at a fixed $B = 0$. Black curve is the zero-field Mattis-Bardeen expectation with no free parameters [41]. (b) Relative dissipation, δQ_i^{-1} , as a function of magnetic field and temperature. B^* indicates the inferred crossover to Bogoliubov-Fermi arcs from Fig. 3.

future work. In practice, the relatively small value of g_y obtained from the fit leads to the absence of Bogoliubov-Fermi arcs in this region, which effectively masks the role of the unstable region for current experimental parameters.

To test the origin of the anisotropic response, we have fabricated two additional samples on 90° rotated crystal axes, and found that the anisotropic circuit response is 90° rotated as well [41]. This shows that the origin of anisotropy is associated with the crystal, consistent with an anisotropic g tensor. It is not currently possible to quantitatively study these orientations because the 90° rotated devices strongly sample the unstable region in the currently available $p \pm ip$ theory. Thus, constructing a more general theory of the induced $p \pm ip$ superfluid response is an outstanding theoretical challenge which must be overcome to analyze all sample orientations.

An additional check of the $p \pm ip$ picture is given by circuit dissipation. The circuit's inverse quality-factor Q_i^{-1} increases abruptly at the characteristic field B^* [Fig. 5(a)], signaling the onset of enhanced dissipation. Currently available theory does not include disorder in the InAs, so is unable to make predictions for dissipation signatures of Bogoliubov-Fermi arcs. We therefore introduce the model-independent dissipation metric

$$\delta Q_i^{-1}(B, T) = Q_i(B, T)^{-1} - Q_i(0, T)^{-1}. \quad (3)$$

δQ_i^{-1} represents an inference of the enhanced dissipation due to magnetic field, covering both the high-temperature limit where $Q_i(0, T)^{-1}$ approaches the Mattis-Bardeen prediction [Fig. 5(a), black], and the low-temperature limit where $Q_i(0, T)^{-1}$ saturates, presumably due to generic effects such as material imperfections. Experimentally mapping δQ_i^{-1} as a function of magnetic field and temperature confirms that there is a generic increase in dissipation for $B > B^*$. The behavior of δQ_i^{-1} bares a striking

resemblance to the behavior of n_p in Figs. 3(c) and 3(d), suggesting the straightforward physical interpretation that the emergence of Bogoliubov-Fermi arcs introduces excess dissipation in the resonator. Such dissipation is different from the usual Fermi liquid, since carriers have a continuously variable charge which depends on both their momentum and magnetic field, highlighting the need for development of a theoretical description.

Summarizing, we have studied the magnetic field and temperature dependence of an Al-InAs superconducting resonator, observing strong departures from the s -wave theory, and good agreement with a theory including the effect of $p \pm ip$ induced superconductivity in the InAs. Within this picture, a sufficiently strong magnetic field induces an anisotropic response and leads to the emergence of Bogoliubov-Fermi surfaces, which result in a rapid shift of the frequency of the resonator and cause sharp onset of excess dissipation. We have considered other origins of the decreased superfluid density. A pure induced s -wave pairing in the InAs is unable to account for our observations [41]. Another scenario is that, despite the careful magnetic-field alignment and lack of contribution below B^* , there is a depinning transition of vortices [72]. The absence of extra frequency shifts below B^* , the weak temperature dependence above B^* [74], and the isotropic response of control samples without an InAs heterostructure [41] all point against this scenario. Anomalous field dependence has been observed in Nb thin films in prior work [75]; we have verified this is not the case for our films [41].

Looking ahead, our technique can now be used to study the properties of different hybrid systems, and to explore alternative geometries that could use Bogoliubov-Fermi surfaces to generate topological phases [76]. During preparation we became aware of a related result reporting Bogoliubov-Fermi surfaces [77].

M. S. acknowledges useful discussions with A. Levchenko and P. A. Lee, and E. Berg. This research was supported by the Scientific Service Units of IST Austria through resources provided by the MIBA Machine Shop and the nanofabrication facility. J. S. and A. G. acknowledge funding from the European Union's Horizon 2020 research and innovation program under the Marie Skłodowska-Curie Grant Agreement No. 754411. W. M. Hatefipour, W. M. Strickland and J. Shabani acknowledge funding from Office of Naval Research Award No. N00014-21-1-2450.

*andrew.higginbotham@ist.ac.at

- [1] R. Yan, G. Khalsa, S. Vishwanath, Y. Han, J. Wright, S. Rouvimov, D. S. Katzer, N. Nepal, B. P. Downey, D. A. Muller, H. G. Xing, D. J. Meyer, and D. Jena, *Nature (London)* **555**, 183 (2018).
- [2] F. Wen, J. Yuan, K. S. Wickramasinghe, M. William, J. Shabani, and E. Tutuc, *IEEE Trans. Electron Devices* **68**, 1524 (2021).

- [3] T. W. Larsen, K. D. Petersson, F. Kuemmeth, T. S. Jespersen, P. Krogstrup, J. Nygård, and C. M. Marcus, *Phys. Rev. Lett.* **115**, 127001 (2015).
- [4] G. de Lange, B. van Heck, A. Bruno, D. J. van Woerkom, A. Geresdi, S. R. Plissard, E. P. A. M. Bakkers, A. R. Akhmerov, and L. DiCarlo, *Phys. Rev. Lett.* **115**, 127002 (2015).
- [5] L. Casparis, T. W. Larsen, M. S. Olsen, F. Kuemmeth, P. Krogstrup, J. Nygård, K. D. Petersson, and C. M. Marcus, *Phys. Rev. Lett.* **116**, 150505 (2016).
- [6] L. Casparis, M. R. Connolly, M. Kjaergaard, N. J. Pearson, A. Kringhøj, T. W. Larsen, F. Kuemmeth, T. Wang, C. Thomas, S. Gronin, G. C. Gardner, M. J. Manfra, C. M. Marcus, and K. D. Petersson, *Nat. Nanotechnol.* **13**, 915 (2018).
- [7] L. Fu and C. L. Kane, *Phys. Rev. Lett.* **100**, 096407 (2008).
- [8] S. Fujimoto, *Phys. Rev. B* **77**, 220501(R) (2008).
- [9] C. Zhang, S. Tewari, R. M. Lutchyn, and S. Das Sarma, *Phys. Rev. Lett.* **101**, 160401 (2008).
- [10] K. Flensberg, F. von Oppen, and A. Stern, *Nat. Rev. Mater.* **6**, 944 (2021).
- [11] V. Mourik, K. Zuo, S. M. Frolov, S. R. Plissard, E. P. A. M. Bakkers, and L. P. Kouwenhoven, *Science* **336**, 1003 (2012).
- [12] E. J. H. Lee, X. Jiang, M. Houzet, R. Aguado, C. M. Lieber, and S. De Franceschi, *Nat. Nanotechnol.* **9**, 79 (2014).
- [13] R. M. Lutchyn, E. P. A. M. Bakkers, L. P. Kouwenhoven, P. Krogstrup, C. M. Marcus, and Y. Oreg, *Nat. Rev. Mater.* **3**, 52 (2018).
- [14] J. Chen, B. D. Woods, P. Yu, M. Hocevar, D. Car, S. R. Plissard, E. P. A. M. Bakkers, T. D. Stanescu, and S. M. Frolov, *Phys. Rev. Lett.* **123**, 107703 (2019).
- [15] P. Yu, J. Chen, M. Gomanko, G. Badawy, E. P. A. M. Bakkers, K. Zuo, V. Mourik, and S. M. Frolov, *Nat. Phys.* **17**, 482 (2021).
- [16] M. Valentini, F. Peñaranda, A. Hofmann, M. Brauns, R. Hauschild, P. Krogstrup, P. San-Jose, E. Prada, R. Aguado, and G. Katsaros, *Science* **373**, 82 (2021).
- [17] S. Hart, H. Ren, M. Kosowsky, G. Ben-Shach, P. Leubner, C. Brüne, H. Buhmann, L. W. Molenkamp, B. I. Halperin, and A. Yacoby, *Nat. Phys.* **13**, 87 (2017).
- [18] H. Ren, F. Pientka, S. Hart, A. T. Pierce, M. Kosowsky, L. Lunczer, R. Schlereth, B. Scharf, E. M. Hankiewicz, L. W. Molenkamp, B. I. Halperin, and A. Yacoby, *Nature (London)* **569**, 93 (2019).
- [19] A. Fornieri, A. M. Whiticar, F. Setiawan, E. Portolés, A. C. C. Drachmann, A. Keselman, S. Gronin, C. Thomas, T. Wang, R. Kallaher, G. C. Gardner, E. Berg, M. J. Manfra, A. Stern, C. M. Marcus, and F. Nichele, *Nature (London)* **569**, 89 (2019).
- [20] M. C. Dartiailh, W. Mayer, J. Yuan, K. S. Wickramasinghe, A. Matos-Abiague, I. Žutić, and J. Shabani, *Phys. Rev. Lett.* **126**, 036802 (2021).
- [21] B. S. Chandrasekhar, *Appl. Phys. Lett.* **1**, 7 (1962).
- [22] A. M. Clogston, *Phys. Rev. Lett.* **9**, 266 (1962).
- [23] S. Tewari, T. D. Stanescu, J. D. Sau, and S. D. Sarma, *New J. Phys.* **13**, 065004 (2011).
- [24] N. F. Q. Yuan and L. Fu, *Phys. Rev. B* **97**, 115139 (2018).
- [25] J. Alicea, *Phys. Rev. B* **81**, 125318 (2010).
- [26] M. Sato and S. Fujimoto, *Phys. Rev. B* **79**, 094504 (2009).
- [27] P. A. Lee, [arXiv:0907.2681](https://arxiv.org/abs/0907.2681).
- [28] J. D. Sau, S. Tewari, R. M. Lutchyn, T. D. Stanescu, and S. Das Sarma, *Phys. Rev. B* **82**, 214509 (2010).
- [29] R. M. Lutchyn, J. D. Sau, and S. Das Sarma, *Phys. Rev. Lett.* **105**, 077001 (2010).
- [30] Y. Oreg, G. Refael, and F. von Oppen, *Phys. Rev. Lett.* **105**, 177002 (2010).
- [31] N. Read and D. Green, *Phys. Rev. B* **61**, 10267 (2000).
- [32] A. C. Potter and P. A. Lee, *Phys. Rev. B* **83**, 184520 (2011).
- [33] W. V. Liu and F. Wilczek, *Phys. Rev. Lett.* **90**, 047002 (2003).
- [34] S.-T. Wu and S. Yip, *Phys. Rev. A* **67**, 053603 (2003).
- [35] M. M. Forbes, E. Gubankova, W. V. Liu, and F. Wilczek, *Phys. Rev. Lett.* **94**, 017001 (2005).
- [36] D. F. Agterberg, P. M. R. Brydon, and C. Timm, *Phys. Rev. Lett.* **118**, 127001 (2017).
- [37] C. Setty, Y. Cao, A. Kreisel, S. Bhattacharyya, and P. J. Hirschfeld, *Phys. Rev. B* **102**, 064504 (2020).
- [38] J. Shabani, M. Kjaergaard, H. J. Suominen, Y. Kim, F. Nichele, K. Pakrouski, T. Stankevic, R. M. Lutchyn, P. Krogstrup, R. Feidenhans'l, S. Kraemer, C. Nayak, M. Troyer, C. M. Marcus, and C. J. Palmstrøm, *Phys. Rev. B* **93**, 155402 (2016).
- [39] M. Kjaergaard, F. Nichele, H. J. Suominen, M. P. Nowak, M. Wimmer, A. R. Akhmerov, J. A. Folk, K. Flensberg, J. Shabani, C. J. Palmstrøm, and C. M. Marcus, *Nat. Commun.* **7**, 12841 (2016).
- [40] W. Mayer, J. Yuan, K. S. Wickramasinghe, T. Nguyen, M. C. Dartiailh, and J. Shabani, *Appl. Phys. Lett.* **114**, 103104 (2019).
- [41] See Supplemental Material at <http://link.aps.org/supplemental/10.1103/PhysRevLett.128.107701> for further information on analysis procedures, experimental details, and theoretical model, which includes Ref.'s [42–55].
- [42] Y. A. Nefyodov, A. V. Shchepetilnikov, I. V. Kukushkin, W. Dietsche, and S. Schmult, *Phys. Rev. B* **84**, 233302 (2011).
- [43] M. D. Schroer, K. D. Petersson, M. Jung, and J. R. Petta, *Phys. Rev. Lett.* **107**, 176811 (2011).
- [44] C. Holloway and E. Kuester, *IEEE Trans. Microwave Theory Tech.* **43**, 2695 (1995).
- [45] A. I. Larkin and Y. N. Ovchinnikov, *Zh. Eksp. Teor. Fiz.* **47**, 1136 (1964).
- [46] P. Fulde and R. A. Ferrell, *Phys. Rev.* **135**, A550 (1964).
- [47] A. A. Abrikosov and L. P. Gor'kov, *Sov. Phys. JETP* **12**, 1243 (1961).
- [48] K. Maki, *Superconductivity*, edited by R. D. Parks (Dekker, New York, 1969), Vol. II.
- [49] K. Maki, *Prog. Theor. Phys.* **31**, 731 (1964).
- [50] R. Thompson and A. Baratoff, *Phys. Rev. Lett.* **15**, 971 (1965).
- [51] K. Maki and T. Tsuneto, *Prog. Theor. Phys.* **31**, 945 (1964).
- [52] S. B. Nam, *Phys. Rev.* **156**, 470 (1967).
- [53] O. V. Dimitrova and M. V. Feigel'man, *J. Exp. Theor. Phys. Lett.* **78**, 637 (2003).
- [54] O. Dimitrova and M. V. Feigel'man, *Phys. Rev. B* **76**, 014522 (2007).
- [55] D. C. Mattis and J. Bardeen, *Phys. Rev.* **111**, 412 (1958).
- [56] A. J. Annunziata, D. F. Santavicca, L. Frunzio, G. Catelani, M. J. Rooks, A. Frydman, and D. E. Prober, *Nanotechnology* **21**, 445202 (2010).

- [57] E. F. C. Driessen, P. C. J. J. Coumou, R. R. Tromp, P. J. de Visser, and T. M. Klapwijk, *Phys. Rev. Lett.* **109**, 107003 (2012).
- [58] S. Probst, F. B. Song, P. A. Bushev, A. V. Ustinov, and M. Weides, *Rev. Sci. Instrum.* **86**, 024706 (2015).
- [59] M. Göppl, A. Fragner, M. Baur, R. Bianchetti, S. Filipp, J. M. Fink, P. J. Leek, G. Puebla, L. Steffen, and A. Wallraff, *J. Appl. Phys.* **104**, 113904 (2008).
- [60] C. Reeg, D. Loss, and J. Klinovaja, *Phys. Rev. B* **97**, 165425 (2018).
- [61] C. Reeg, D. Loss, and J. Klinovaja, *Beilstein J. Nanotechnol.* **9**, 1263 (2018).
- [62] A. E. G. Mikkelsen, P. Kotetes, P. Krogstrup, and K. Flensberg, *Phys. Rev. X* **8**, 031040 (2018).
- [63] A. E. Antipov, A. Bargerbos, G. W. Winkler, B. Bauer, E. Rossi, and R. M. Lutchyn, *Phys. Rev. X* **8**, 031041 (2018).
- [64] T. Kiendl, F. von Oppen, and P. W. Brouwer, *Phys. Rev. B* **100**, 035426 (2019).
- [65] C. H. Möller, C. Heyn, and D. Grundler, *Appl. Phys. Lett.* **83**, 2181 (2003).
- [66] J. Nitta, Y. Lin, T. Akazaki, and T. Koga, *Appl. Phys. Lett.* **83**, 4565 (2003).
- [67] Y. V. Terent'ev, S. N. Danilov, M. V. Durnev, J. Loher, D. Schuh, D. Bougeard, S. V. Ivanov, and S. D. Ganichev, *J. Appl. Phys.* **121**, 053904 (2017).
- [68] J. Yuan, M. Hatefipour, B. A. Magill, W. Mayer, M. C. Dartailh, K. Sardashti, K. S. Wickramasinghe, G. A. Khodaparast, Y. H. Matsuda, Y. Kohama, Z. Yang, S. Thapa, C. J. Stanton, and J. Shabani, *Phys. Rev. B* **101**, 205310 (2020).
- [69] V. Kalevich and V. Korenev, *JETP Lett.* **56**, 253 (1992).
- [70] V. K. Kalevich and V. L. Korenev, *JETP Lett.* **57**, 571 (1993).
- [71] P. S. Eldridge, J. Hübner, S. Oertel, R. T. Harley, M. Henini, and M. Oestreich, *Phys. Rev. B* **83**, 041301(R) (2011).
- [72] Al is a type-I superconductor, but in the thin film limit has a field-dependent behavior similar to a type-II [73].
- [73] C. Song, T. W. Heitmann, M. P. DeFeo, K. Yu, R. McDermott, M. Neeley, J. M. Martinis, and B. L. T. Plourde, *Phys. Rev. B* **79**, 174512 (2009).
- [74] R. Prozorov and R. W. Giannetta, *Supercond. Sci. Technol.* **19**, R41 (2006).
- [75] G. Allison, A. Oiwa, S. Kumar, D. DiVincenzo, M. Ketchen, K. Hirakawa, H. Takayanagi, and S. Tarucha, *J. Phys.* **245**, 012024 (2010).
- [76] M. Papaj and L. Fu, *Nat. Commun.* **12**, 577 (2021).
- [77] Z. Zhu, M. Papaj, X.-A. Nie, H.-K. Xu, Y.-S. Gu, X. Yang, D. Guan, S. Wang, Y. Li, C. Liu, J. Luo, Z.-A. Xu, H. Zheng, L. Fu, and J.-F. Jia, *Science* **374**, 1381 (2021).